

A microfocus X-ray fluorescence beamline at Indus-2 synchrotron radiation facility

M. K. Tiwari,* P. Gupta, A. K. Sinha, S. R. Kane, A. K. Singh, S. R. Garg, C. K. Garg, G. S. Lodha and S. K. Deb

Indus Synchrotrons Utilisation Division, Raja Ramanna Centre for Advanced Technology, Indore, MP 452013, India. E-mail: mktiwari@rrcat.gov.in

A microfocus X-ray fluorescence spectroscopy beamline (BL-16) at the Indian synchrotron radiation facility Indus-2 has been constructed with an experimental emphasis on environmental, archaeological, biomedical and material science applications involving heavy metal speciation and their localization. The beamline offers a combination of different analytical probes, *e.g.* X-ray fluorescence mapping, X-ray microspectroscopy and total-external-reflection fluorescence characterization. The beamline is installed on a bending-magnet source with a working X-ray energy range of 4–20 keV, enabling it to excite *K*-edges of all elements from S to Nb and *L*-edges from Ag to U. The optics of the beamline comprises of a double-crystal monochromator with Si(111) symmetric and asymmetric crystals and a pair of Kirkpatrick–Baez focusing mirrors. This paper describes the performance of the beamline and its capabilities with examples of measured results.

© 2013 International Union of Crystallography
Printed in Singapore – all rights reserved

Keywords: X-ray microscopy; microprobe; X-ray fluorescence; X-ray scattering.

1. Introduction

X-ray fluorescence spectrometry is a powerful non-destructive technique for the elemental analysis of materials at the micro and trace level. The technique finds applications in a variety of fields (*viz.* geology, archaeology, biomedical science and material science, *etc.*). Apart from the research applications, the technique has potential usages in industry, especially in maintaining quality control of ultra-pure chemical reagents and products. Over the past two decades X-ray beams produced from various focusing optics such as Kirkpatrick–Baez (KB) optics, compound refractive lens, capillary optics, nano-collimators and X-ray waveguide structures (Kirkpatrick & Baez, 1948; Tomie, 2010; Lagomarsino *et al.*, 1997; Jark *et al.*, 2001; Evans-Lutterodt *et al.*, 2003) have led to many interesting applications such as X-ray fluorescence microscopy, microtomography, X-ray imaging, X-ray reflectivity and scattering measurements (Di Fonzo *et al.*, 2000; Drakopoulos *et al.*, 2002; Cedola *et al.*, 2003; Reichert *et al.*, 2003; Alianelli *et al.*, 2009; Tiwari *et al.*, 2010).

Considering the numerous advantages of the synchrotron-based microfocus-X-ray fluorescence (μ -XRF) technique (Iida & Noma, 1993; Newville *et al.*, 1999; Bertrand *et al.*, 2003; Marcus *et al.*, 2004; Somogyi *et al.*, 2005; Mosselmans *et al.*, 2009; Tancharakorn *et al.*, 2012) and to fulfil the requirements of the XRF spectroscopy users of universities and various research laboratories in India, we have built a μ -XRF beamline (BL-16) at the Indus-2 synchrotron radiation source. The beamline is installed on a bending-magnet source and works in the X-ray energy range 4–20 keV. It provides both micro-focused and collimated beam modes at the experimental station. Using the microfocused mode of the beamline, it is possible to examine a specimen for spatial distribution of elements. The beamline allows a user to perform energy-dispersive X-ray fluorescence

analysis and total-reflection X-ray fluorescence characterization of materials at p.p.b. (parts per billion) levels. Apart from the elemental mapping, the beamline also offers other modes of XRF characterization, *viz.* grazing-incidence X-ray fluorescence analysis of thin films and surfaces, chemical speciation, and near-edge absorption spectroscopy *etc.*, using the collimated beam mode.

The BL-16 beamline began user operation in mid-2011. Since then it has been used for a variety of user's research applications. In this article, design specifications, various important features and some commissioning results obtained using the μ -XRF beamline on Indus-2 are presented. A summary of the experimental possibilities on the beamline and ancillary equipment for the user community is described.

2. Details of the source and beamline

2.1. Indus-2 source

Indus-2 is a 2.5 GeV, 300 mA third-generation synchrotron radiation source, with a critical wavelength of $\sim 2 \text{ \AA}$ (Sahni, 2009). It comprises of a double-bend-achromat lattice with zero dispersion function along the straight sections. This yields a low-emittance and high-brightness photon source size for the bending magnets. The estimated photon source size (FWHM) for the Indus-2 bending magnets is $\sim 120 \mu\text{m}$ (V) \times $546 \mu\text{m}$ (H) at 10 keV X-ray energy. The Indus-2 is at present operating at 2.5 GeV, 100 mA.

2.2. Beamline description

The microprobe XRF beamline (BL-16) has been installed on the 5° port of a bending magnet. It has been designed to work in the photon energy range 4–20 keV and has an acceptance of 1 mrad (H)

Table 1

Main parameters of the BL-16 beamline.

| | |
|---|--|
| Source | Bending magnet |
| Working energy range | 4–20 keV |
| Beam acceptance | 1 mrad (H) × 0.2 mrad (V) |
| Monochromator | Si (111) double-crystal monochromator |
| Energy resolution | $\sim 10^{-3}$ – 10^{-4} |
| Beam spot size (at the sample position) | ~ 4.3 mm (V) × 7.5 mm (H) (focused mode) ~ 22 mm (H) × 5 mm (V) (collimated beam mode) |
| Photon flux [at 10 keV X-rays (100 mA ring current) ⁻¹] | $\sim 3 \times 10^7$ photons s ⁻¹ (focused mode) $\sim 2 \times 10^8$ photons s ⁻¹ mm ⁻² (collimated mode) |

× 0.2 mrad (V). The main optical components of the beamline are shown in Fig. 1 and include a fixed-exit double-crystal monochromator (DCM) (FMB, Berlin, Germany) with a pair of symmetric and asymmetric Si (111) crystals (mounted side-by-side) and a KB focusing system with a pair of elliptical mirrors. The DCM can use either pair of Si (111) crystals. An asymmetry angle of 5° has been chosen for the asymmetric Si (111) crystals. The selection of asymmetric Si (111) crystals provides ~1.5 to 2 times higher photon flux compared with symmetric Si (111) crystals. The DCM is placed ~19 m from the source and the KB focusing optics is placed ~4.7 m from the DCM. The KB focusing optics (Xradia, USA) comprises a pair of Pt-coated (25 nm) elliptical bendable mirrors. The measured r.m.s. slope errors (tangential) for the two elliptical mirrors were found to be better than ~1.4 μrad whereas r.m.s. surface roughness was observed using the ‘Micromap’ surface profiler instrument (Micromap Corporation) and found to be ~0.3 nm. A more detailed description of the KB optics is given later. In addition, there are several other components such as a water-cooled four-blade slit (S1), an uncooled four-blade slit (S2), fluorescence screens, *etc.*, that complete the optical layout of the beamline. The combination of slits allows shaping of the X-ray beam dimensions that fit to the user’s requirements. The main beamline parameters are summarized in Table 1. The beamline radiation shielding hutch and the built-in personal safety interlock system allow safe operation of the beamline. The beamline operates under high-vacuum conditions ($\sim 1 \times 10^{-6}$ mbar). The experimental stations of the BL-16 beamline consist of a five-axis sample manipulator for microprobe-XRF scanning applications, a two-circle goniometer for total-reflection X-ray fluorescence (TXRF) and X-ray reflectivity measurements. A variety of detectors (ionization chamber, photodiode, Vortex spectroscopy

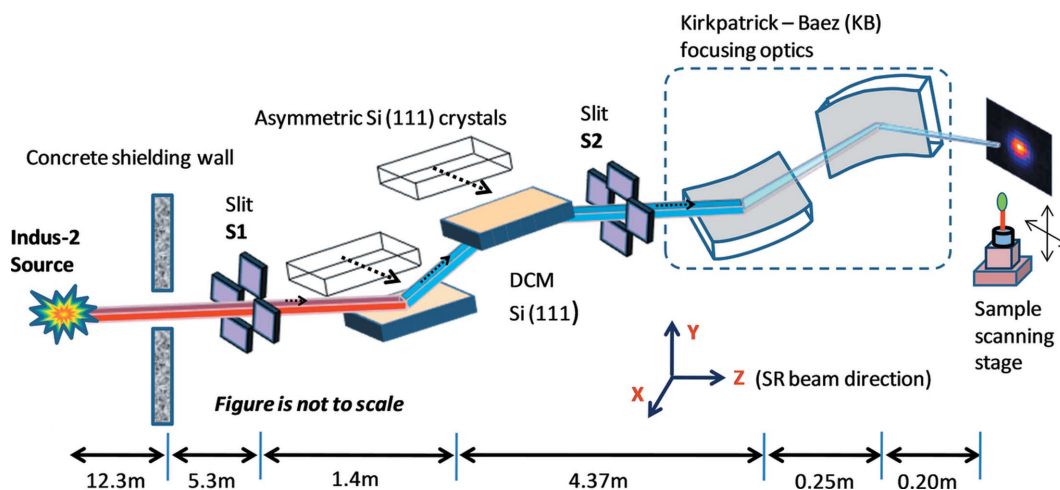
detector and MiniFdi and VHR X-ray CCD cameras) are also available on the beamline making it possible to record good quality data.

3. Results and discussion

In order to determine the characteristics parameters of the beamline such as spectral range, element range and minimum detection sensitivities of various elements, X-ray fluorescence spectra of various standard reference materials (SRMs) (NIST, USA) have been examined for an acquisition time of ~300 s. The XRF spectra were recorded using a Vortex energy-dispersive detector (SII Nano Technology, USA). The detector was placed in the horizontal plane at an angle of ~90° with respect to the incident beam in order to take advantage of the polarization geometry of the synchrotron radiation beam whereas the specimen was placed at ~45° with respect to the incident X-ray beam. An X-ray beam size of ~4 mm × 4 mm was allowed for the sample excitation. Fig. 2 shows the measured fluorescence spectra of various SRMs. The minimum detection limits (MDLs) obtained for different elements using the formalism

$$C_{\text{MDL}} = \frac{3\sqrt{I_B}}{I_A/C_A}, \quad (1)$$

where I_B is the background intensity under the fluorescence peak of the analyte element A , I_A is the net area intensity of the analyte and C_A is the weight concentration of the analyte, are found to be ~200 p.p.b. to 3 p.p.m. for elements of atomic number Z ranging from 22 to 40. These detection sensitivities were derived for a sample-to-detector distance of ~50 mm. Nevertheless, the fluorescence efficiency of an element strongly depends on the excitation energy E_0 ; hence, by properly selecting the excitation energy close to the absorption edge of an element and optimizing the detector-to-sample distance down to ~15 mm, C_{MDL} can be increased further. Another important characteristic parameter of the beamline is the incident photon flux available at the experimental station for sample excitation. The monochromatic photon flux reaching the experimental station of the beamline per mm² area was measured by using a calibrated AXUV 100 photodiode (IRD, USA) and found to be $\sim 10^7$ – 10^8 photons s⁻¹ mm⁻² (100 mA)⁻¹ over most of the X-ray energy range of the beamline.


Figure 1

Schematic optical layout of the X-ray microfocus beamline (BL-16) on the Indus-2 synchrotron radiation facility.

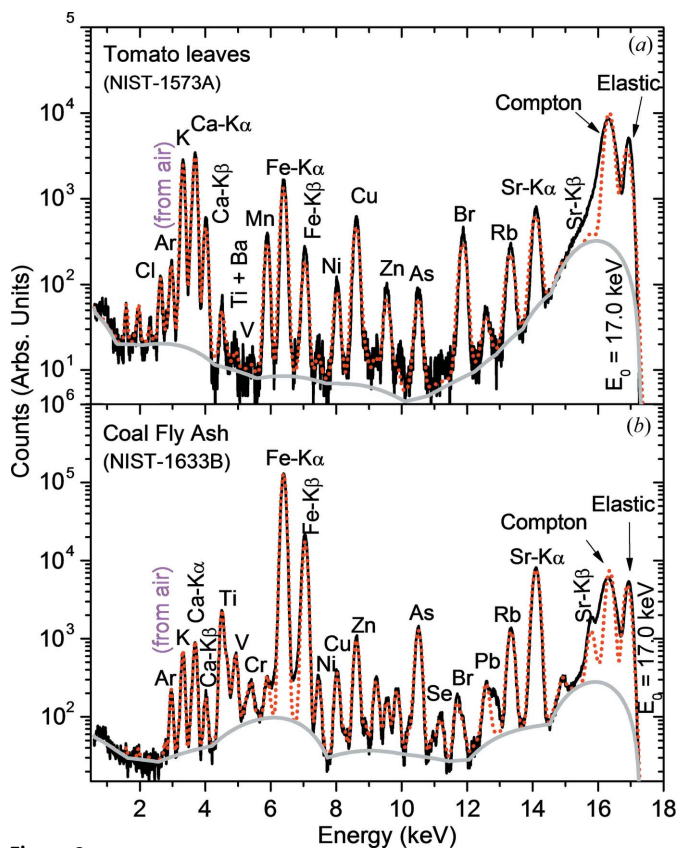


Figure 2 Measured energy-dispersive X-ray fluorescence spectra from different NIST standard reference materials for a spectrum acquisition time of 300 s. Monochromatic X-rays of energy 17.0 keV from a double-crystal monochromator were used as the excitation energy for these NIST standards. (a) Tomato leaves (NIST-1573A), (b) coal fly ash (NIST-1633B). Black solid lines are experimental data, dotted lines are fitted data and the thick grey lines represent an estimation of the spectral background. All the fluorescence measurements were performed in an air environment.

3.1. Microfocus beam

The relative advantages and disadvantages of popular optical schemes for the generation of microfocused beams in synchrotron beamlines have been discussed (Iida & Noma, 1993; Hayakawa *et al.*, 2001). In order to obtain a stable X-ray focal spot over the entire working energy range of the beamline, the microfocus X-ray beam on the BL-16 experimental station uses KB focusing optics. The KB focusing optics includes bendable elliptical mirrors of size ~ 30 mm (W) \times 200 mm (L). The mirrors, as well as the associated motion mechanism (two independent bender actuators on each mirrors, tilt and translation motions for each mirrors), have been mounted inside the KB vacuum chamber housing. The vacuum chamber of the KB system has two beryllium windows of thickness ~ 75 μ m at the entrance and exit ends. It is possible to operate the KB system either in a helium environment or under high-vacuum conditions ($\sim 10^{-6}$ mbar). All the alignment actuators used in the KB optics are picomotor driven and provided with linear variable differential transformer readouts. We have used an uncooled four-blade slit (S2) before the KB optics in order to control the size of the incident beam. We followed standard alignment procedures (Naulleau *et al.*, 2002) to generate a microfocused beam spot from the KB optics. The tilt angles on both the vertical and horizontal mirrors of the KB system have been maintained at ~ 3.9 mrad in order to obtain a focused X-ray beam with a maximum energy of ~ 20 keV. Knife-edge

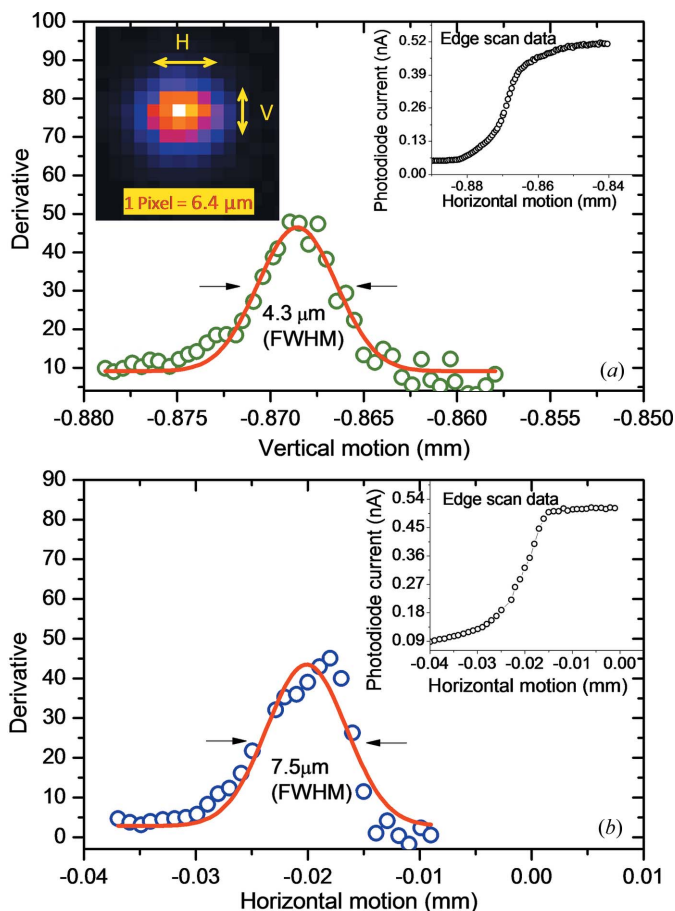


Figure 3 Measured vertical (a) and horizontal (b) profiles of the microfocused beam obtained using a knife-edge scan set-up giving a focus beam of size ~ 4.3 μ m (V) \times 7.5 μ m (H). The open circles are the measured data whereas solid lines are the fitted Gaussian profiles. The inset shows the recorded CCD image of the optimized microfocused beam generated from the KB system at the BL-16 experimental station.

measurements were performed to determine the vertical and horizontal dimensions of the microfocused beam. A knife-edge arrangement, consisting of ~ 200 μ m-diameter gold wire mounted in the cross geometry followed by a Si photodiode, was placed at the focal position of the KB optics. The focused beam was scanned with a step of ~ 0.5 μ m in the vertical and horizontal directions. The measured vertical and horizontal profiles of the microfocused beam are shown in Fig. 3. The derivatives of the vertical and horizontal scan profiles provide a focus beam dimension of ~ 4.3 μ m (V) \times 7.5 μ m (H) which was found to match reasonably well with the theoretical expected values [3.2 μ m (V) \times 5 μ m (H)]. The inset of Fig. 3(a) shows a CCD image of the best optimized microfocused beam seen from the KB optics. The measured photon flux in the microfocused beam was found to be one order of magnitude less [$\sim 10^6$ – 10^7 photons s^{-1} (100 mA) $^{-1}$] compared with the collimated beam flux.

3.2. Microfluorescence mapping

The BL-16 beamline has been used for microfluorescence measurements of a variety of heterogeneous multi-element samples (Misra *et al.*, 2013). In a case study, the microfluorescence mapping capabilities of the beamline have been examined by analyzing a Cu grid structure. The grid structure was mounted on a five-axis sample manipulator stage close to the focal distance of the KB system and

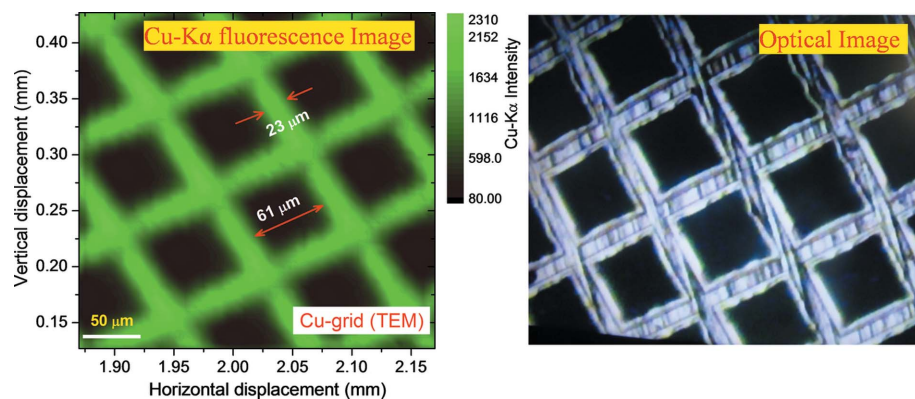


Figure 4
Measured fluorescence micrograph of a Cu grid structure used in transmission electron microscopy using the BL-16 microfocus beam. On the right hand side of the figure an optical image of the Cu grid structures is shown.

then scanned in the XY plane, perpendicular to the synchrotron radiation beam direction in steps of $\sim 5 \mu\text{m}$. At each point the fluorescence spectrum was recorded for an acquisition time of $\sim 5 \text{ s}$. Fig. 4 shows the two-dimensional fluorescence map of the Cu grid generated using Cu $K\alpha$ intensity. The observed dimensions of the Cu grid structure determined from the microfluorescence mapping were found to match closely with the optical measurements.

3.3. X-ray reflectivity and TXRF analysis

The BL-16 beamline also includes a third experimental station that allows users to perform ultra-trace-element analysis using the total-external-reflection X-ray fluorescence technique and microstructural characterization of thin layered materials using X-ray reflectivity measurements. It comprises a two-circle goniometer installed on a vibration-free optics table. To measure the specular reflected X-ray intensity from a flat surface, a scintillator detector is used on the exit arm of the goniometer. In TXRF geometry, it is possible to mount a solid-state energy-dispersive spectroscopy detector either in the plane of the synchrotron radiation beam or perpendicular ($\sim 90^\circ$) to the substrate surface. The determined elemental detection sensitivities in TXRF mode obtained using a standard reference material (NIST-1640: trace elements in natural water) at a monochromatic excitation energy of 15 keV were found to be in the range 1 p.p.b. to ~ 35 p.p.b. for elements of atomic number Z ranging from 16 to 34. Additional details of the experimental station are given elsewhere (Tiwari, 2012).

4. Summary

The design, construction and realisation of a microprobe X-ray fluorescence beamline on the Indus-2 synchrotron radiation facility is presented. The BL-16 beamline allows various re-configurable operational modes (normal XRF, TXRF and μ -XRF modes) with a minimal set-up time which enables a wide range of experiments to be performed. It is possible to collect high-quality XRF data, capable of determining the chemical composition, despite the relatively low concentrations of the element of interest present in a specimen. One can record fluorescence micrographs of a sample in order to distinguish any kinds of elemental heterogeneity in a specimen. By virtue of its several operational modes, and different interchangeable instruments available on the beamline, it provides an attractive

platform for researchers at Indian universities to accomplish a variety of research activities especially in the fields of archaeology, earth science and environmental applications, etc.

We would like to acknowledge mechanical assistance from Arjun Kumar, R. K. Solanki and other support groups of Indus Synchrotron Machine for their help in the construction and alignment of the beamline. We are thankful to Dr. P. D. Gupta for his constant encouragement and support during the construction and installation phase of the beamline. Dr K. J. S. Sawhney from Diamond Light Source, UK, is gratefully acknowledged for several fruitful discussions and suggestions.

References

- Alianelli, L., Sawhney, K. J. S., Tiwari, M. K., Dolbnya, I. P., Stevens, R., Jenkins, D. W. K., Loader, I. M., Wilson, M. C. & Malik, A. (2009). *J. Synchrotron Rad.* **16**, 325–329.
- Bertrand, L., Doucet, J., Dumas, P., Simionovici, A., Tsoucaris, G. & Walter, P. (2003). *J. Synchrotron Rad.* **10**, 387–392.
- Cedola, A., Stanic, V., Burghammer, M., Lagomarsino, S., Rustichelli, F., Giardino, R., Nicoli Aldini, N., Fini, M., Komlev, V. & Di Fonzo, S. (2003). *Phys. Med. Biol.* **48**, N37–N48.
- Di Fonzo, S., Jark, W., Lagomarsino, S., Giannini, C., De Caro L., Cedola, A. & Muller, M. (2000). *Nature (London)*, **403**, 638–640.
- Drakopoulos, M., Zegenhagen, J., Snigirev, A., Snigireva, I., Hauser, M., Eberl, K., Aristov, V., Shabelnikov, L. & Yunkin, V. (2002). *Appl. Phys. Lett.* **81**, 2279.
- Evans-Lutterodt, K., Ablett, J., Stein, A., Kao, C. C., Tennant, D., Klemens, F., Taylor, A., Jacobsen, C., Gammel, P., Huggins, H., Bogart, G., Ustin, S. & Ocola, L. (2003). *Opt. Express*, **11**, 919–926.
- Hayakawa, S., Ikuta, N., Suzuki, M., Wakatsuki, M. & Hirokawa, T. (2001). *J. Synchrotron Rad.* **8**, 328–330.
- Iida, A. & Noma, T. (1993). *Nucl. Instrum. Methods Phys. Res. B*, **82**, 129–138.
- Jark, W., Cedola, A., Di Fonzo, S., Fiordelisi, M., Lagomarsino, S., Kovalenko, N. V. & Chernov, V. A. (2001). *Appl. Phys. Lett.* **78**, 1192.
- Kirkpatrick, P. & Baez, A. V. (1948). *J. Opt. Soc. Am.* **38**, 766–774.
- Lagomarsino, S., Cedola, A., Cloetens, P., Di Fonzo, S., Jark, W., Soullié, G. & Riekel, C. (1997). *Appl. Phys. Lett.* **71**, 2557.
- Marcus, M. A., MacDowell, A. A., Celestre, R., Manceau, A., Miller, T., Padmore, H. A. & Sublett, R. E. (2004). *J. Synchrotron Rad.* **11**, 239–247.
- Misra, N. L., Tiwari, M. K., Sanjay Kumar, S., Dhara, S., Singh, A. K., Lodha, G. S., Deb, S. K., Gupta, P. D. & Aggarwal, S. K. (2013). *X-ray Spectrom.* **42**, 4–7.
- Mosselmans, J. F. W., Quinn, P. D., Dent, A. J., Cavill, S. A., Moreno, S. D., Peach, A., Leicester, P. J., Keylock, S. J., Gregory, S. R., Atkinson, K. D. & Rosell, J. R. (2009). *J. Synchrotron Rad.* **16**, 818–824.
- Naulleau, P. P., Batson, P., Denham, P., Richardson, D. & Underwood, J. (2002). *Opt. Commun.* **212**, 225–233.
- Newville, M., Sutton, S. R., Rivers, M. L. & Eng, P. (1999). *J. Synchrotron Rad.* **6**, 353–355.
- Reichert, H., Honkimäki, V., Snigirev, A., Engemann, S. & Dosch, H. (2003). *Physica B*, **336**, 46–55.
- Sahni, V. C. (2009). *AIP Conf. Proc.* **1150**, 180–187.
- Somogyi, A., Tucoulou, R., Martinez-Criado, G., Homs, A., Cauzid, J., Bleuett, P., Bohic, S. & Simionovici, A. (2005). *J. Synchrotron Rad.* **12**, 208–215.
- Tancharakorn, S., Tanthanuch, W., Kamonsutthipajit, N., Wongprachanukul, N., Sophon, M., Chaichuay, S., Uthaisar, C. & Yimnirun, R. (2012). *J. Synchrotron Rad.* **19**, 536–540.
- Tiwari, M. K. (2012). *RRCAT NewsL.* **25**, 5.
- Tiwari, M. K., Alianelli, L., Dolbnya, I. P. & Sawhney, K. J. S. (2010). *J. Synchrotron Rad.* **17**, 237–242.
- Tomie, T. (2010). *Spectrochim. Acta Part B*, **65**, 192–198.